Eur. Phys. J. Spec. Top. (2021) 230:551–559
https://doi.org/10.1140/epjs/s11734-021-00004-4

THE EUROPEAN PHYSICAL JOURNAL SPECIAL TOPICS

Regular Article

Finding quark content of neutron stars in light of GW170817

Rana Nandi[1,a] and Subrata Pal[2]

[1] Polba Mahavidyalaya, Hooghly, West Bengal 712148, India
[2] Department of Nuclear and Atomic Physics, Tata Institute of Fundamental Research, Mumbai 400005, India

Received 17 June 2020 / Accepted 23 December 2020 / Published online 29 March 2021

Abstract The detection of gravitational waves from GW170817 has provided a new opportunity to constrain the equation of state (EOS) of neutron stars. In this article, we investigate the possible existence of quarks inside the neutron star core in the context of GW170817. The nucleon phase is treated within the relativistic nuclear mean-field approach where we have employed a fully comprehensive set of available models, and the quark phase is described in the Bag model. We show that the nucleonic EOSs which are inconsistent with the tidal deformability bound become consistent when phase transition to quark matter via Gibbs construction is allowed. We find that several nucleonic EOSs support the presence of pure quark matter core with a small mass not more than $0.17M_\odot$ confined within a radius of 0.9 km. We also find that the strong correlation between tidal deformability and neutron star radii observed for pure nucleonic stars does persist even with a nucleon-quark phase transition and provides an upper limit on the radius of $R_{1.4} \lesssim 12.9$ km for a $1.4M_\odot$ neutron star.

1 Introduction

Neutron stars (NSs) are highly compact astrophysical objects which are produced at the end of the life cycles of massive stars ($8M_\odot \lesssim M \lesssim 25M_\odot$) via supernova explosions. A NS can have mass between $\sim 1{-}2M_\odot$, but with a rather small radius of only between 10 and 15 km. As a result, the density inside the star can be very high $\sim 10^{15}{-}10^{16}$ g/cm^3, which is several times larger than the saturation density ($\rho_0 \sim 2.8 \times 10^{14}$) g/cm^3 of nuclear matter [1]. The state of the matter, i.e. the equation of state (EOS) and the composition, is not known at such high densities as laboratory experiments and ab initio calculations can only provide description of nuclear matter at around the saturation density. The high-density EOS of NS matter is thus highly uncertain and it is explored by adopting different models [2].

To reliably constrain the EOS, one should rely on astrophysical observations [3]. Given an EOS, the Tolman–Oppenheimer–Volkoff equations provide an unique sequence of masses and radii for NS with the sequence terminating at a maximum mass $M_{\rm max}$. The value of $M_{\rm max}$ depends on the stiffness of the EOS, i.e. how rapidly the pressure increases with the energy density, and a stiffer EOS generates a larger maximum mass star. Of course, the larger matter pressure in a stiffer EOS state also generates stars with larger radii. Thus measurements of masses and radii of NSs can put significant constraint on the EOS [4].

The appearance of new degrees of freedom, such as quarks inside the core of neutron star, would soften the overall EOS resulting in decrease of maximum mass and radius. In fact, the deconfinement transition from hadron to quark-gluon phase, as predicted in the theory of strong interactions—quantum chromodynamics, has been already observed at high temperature and small net-baryon density in ultra-relativistic heavy ion collisions. In contrast, the presence of quark matter inside the high-density core of neutron stars still remains a open question. By combining astrophysical observations of mass and radii of neutron stars with various theoretical models of strongly interacting matter, one can provide empirical constraints on the quark-matter content inside stars.

The first major observational breakthrough in this direction came with the precise measurement of masses of two massive NS with masses of $(1.928 \pm 0.017)M_\odot$ [5,6] and $(2.01 \pm 0.04M_\odot)$ [7]. Very recently, another massive NS of mass $2.14^{+0.20}_{-0.18}$ within 95.4% credibility interval ($2.14^{+0.10}_{-0.09}$, within 68.3% credibility interval) has been detected [8]. These measurements will essentially exclude the soft EOSs for which $M_{\rm max} < 1.97M_\odot$. In fact, to determine the EOS uniquely one also requires precise measurements of radius of stars. A few measurements have been performed for NS radii from quiescent low-mass X-ray binaries and from the thermonuclear bursts of accreting NS [9–12]. Although these

[a] e-mail: nandi.rana@gmail.com (corresponding author)

measurements are important, but these are unable to impose significant constraint on the EOS as the uncertainty is quite large of $\sim 11-29\%$. NASA's *Neutron Star Interior Composition Explorer (NICER)* instrument was installed on the International Space Station on 2017 with the mission partly to measure the masses and radii of NS within $\sim 5\%$ uncertainty. Recently, NICER collaboration has estimated [13,14] the mass ($M = 1.34^{+0.15}_{-0.16} M_\odot$) and radius ($R = 12.71^{+1.14}_{-1.19}$ km) of the millisecond pulsar PSR J0030+0451.

On August 2017, LIGO-Virgo Collaboration (LVC) detected first ever gravitational waves from the binary NS merger event GW170817 [15]. This historic detection has opened up a new avenue to constrain the EOS at high densities. During the inspiral phase of a binary NS merger the strong gravitational field of each star tidally deform the other leaving detectable imprint in the emitted gravitational wave signal [16]. By analyzing the data of GW170817, LVC obtained an upper bound on the tidal deformability of a $1.4M_\odot$ neutron star of $\Lambda_{1.4} \leq 800$. Due to its strong sensitivity on the radius ($\Lambda \sim R^5$), tidal deformability can put stringent constraint on the EOS. Subsequently, several studies were carried out to constrain the EOS [17–21] using the tidal deformability bound provided by GW170817. These studies provided an upper bound on the radius of a $1.4M_\odot$ neutron star of $R_{1.4} \lesssim 13.5-13.8$ km [17–21]. Upper bounds on the maximum mass $M_{\rm max} \lesssim 2.2M_\odot$ were also obtained by several authors by analyzing the data of gravitational wave signal as well as the electromagnetic counterparts of GW170817 [22–24]. Both these bounds imply that the EOS cannot be very stiff. Later LVC improved their analysis of GW170817 data by assuming a common EOS for both the stars and improved waveform model and obtained $\Lambda_{1.4} = 190^{+290}_{-120}$, which translates to an more stringent upper bound of $\Lambda_{1.4} \leq 580$ [25].

Recently, we performed an extensive analysis of the widely used relativistic mean-field (RMF) model EOSs using the observational constraints on the maximum mass of neutron star and tidal deformability of GW170817 and also employing the latest bounds on the saturation properties of nuclear matter [26]. We found that only 3 out of 269 RMF model EOSs are consistent with all the constraints. Using a few selected nucleonic EOSs and limited range of quark matter parameters, we further showed that if the phase transition from nucleonic matter to quark matter via Gibbs construction is incorporated in the EOS at higher density, several EOSs become consistent with all the observational bounds [20,26]. In this article, we shall make a comprehensive analysis of the properties of the neutron star with a nucleon-quark first-order phase transition. For this purpose, we shall employ all the available nuclear RMF models for the nucleon sector and the Bag model for the quark sector where the Bag model parameters are allowed to encompass the entire permissible range of the quark matter parameter space. We shall show that majority of the pure nucleonic model EOSs, which are consistent with the neutron star maximum mass bound of $M_{\rm max} \geq 1.97M_\odot$, do not satisfy the tidal deformability bound of $\Lambda_{1.4} \leq 580$ [25]. Inclusion of a quark phase in the neutron star softens the overall EOS, and we find that these stars become consistent with the tidal deformability bound for realistic values of Bag model parameter space. We shall also show that pure quark matter, though of small mass, can exist in the core of neutron stars.

The article is organized as follows. In Sect. 2, we provide the details of EOS calculation for both the nucleonic phase and the quark phase. In Sect. 3, we present the results for the maximum mass and radii of pure nucleon stars and with nucleon-quark phase transition. We discuss the resulting implications on the composition and content of quark matter in light of maximum mass and tidal deformability constraints. Finally, in Sect. 4, we conclude with a discussion.

2 Setup

In this section, we discuss the construction of EOSs for both the nucleonic matter and quark matter and the phase transition between them. We also discuss the calculation of tidal deformability of neutron stars.

2.1 Nucleonic EOS

We construct the EOS of the nuclear matter containing neutrons, protons, electrons and muons by adopting RMF approach introduced by Walecka [27] and refined over the years by many authors [28–32]. In this model, the interactions between nucleons are described via the exchange of several mesons. The most general form of the Lagrangian can be written as [33]

$$\begin{aligned}
\mathcal{L} = \sum_N \bar{\psi}_N \Big[& \gamma^\mu \left(i\partial_\mu - g_\omega \omega_\mu - \frac{1}{2} g_\rho \boldsymbol{\tau} \cdot \boldsymbol{\rho_\mu} \right) \\
& - (m_N - g_\sigma \sigma - g_\delta \boldsymbol{\tau} \cdot \boldsymbol{\delta})\Big] \psi_N \\
& + \frac{1}{2} \left(\partial_\mu \sigma \partial^\mu \sigma - m_\sigma^2 \sigma^2 \right) - \frac{\kappa}{3!} (g_\sigma \sigma)^3 - \frac{\lambda}{4!} (g_\sigma \sigma)^4 \\
& - \frac{1}{4} \omega_{\mu\nu} \omega^{\mu\nu} + \frac{1}{2} m_\omega^2 \omega_\mu \omega^\mu + \frac{\zeta}{4!} (g_\omega^2 \omega_\mu \omega^\mu)^2 \\
& - \frac{1}{4} \boldsymbol{\rho_{\mu\nu}} \cdot \boldsymbol{\rho^{\mu\nu}} + \frac{1}{2} m_\rho^2 \boldsymbol{\rho_\mu} \cdot \boldsymbol{\rho^\mu} + \frac{1}{2} \left(\partial^\mu \boldsymbol{\delta} \cdot \partial_\mu \boldsymbol{\delta} - m_\delta \boldsymbol{\delta^2} \right) \\
& + g_\sigma g_\omega^2 \sigma \omega_\mu \omega^\mu \left(\alpha_1 + \frac{1}{2} \alpha_1' \right) \\
& + g_\sigma g_\rho^2 \sigma \boldsymbol{\rho_\mu} \cdot \boldsymbol{\rho^\mu} \left(\alpha_2 + \frac{1}{2} \alpha_2' \right) \\
& + \frac{1}{2} \alpha_3' g_\omega^2 g_\rho^2 \omega_\mu \omega^\mu \boldsymbol{\rho_\mu} \cdot \boldsymbol{\rho^\mu}, \qquad (1)
\end{aligned}$$

where ψ_N is the isospin doublet of nucleons, σ, ω, ρ and δ represent scalar-isoscalar, vector-isoscalar, vector-isovector and scalar-isovector meson fields, respectively. There are another class of RMF models, where the nucleon–meson couplings are not constants but density

dependent [34,35] and they do not contain any self-coupling or cross-coupling terms of mesons.

Some of the parameters appearing in the Lagrangian are determined by fitting to the known saturation properties of nuclear matter such as binding energy per nucleon, the saturation density, the symmetry energy (J), the incompressibility (K) and the nucleon effective mass (m^*) [1]. Rest of the parameters are essentially free and can be varied to match various nuclear and NS properties. For certain EOSs, the binding energies and charge radii of some finite nuclei are also used to determine the parameters [32,34,36]. Out of 269 RMF parameter sets, only 67 are found [26] consistent with the latest experimental/empirical bounds on the following saturation properties [2]:

$$\begin{aligned} 210 \;&\leq\; K\,(\mathrm{MeV}) \;\leq 280 \\ 28 \;&\leq\; J\,(\mathrm{MeV}) \;\leq 35 \\ 30 \;&\leq\; L\,(\mathrm{MeV}) \;\leq 87. \end{aligned} \tag{2}$$

A wider range than the generally accepted values for incompressibility, namely $K = 248 \pm 8$ MeV [37] or $K = 240 \pm 20$ MeV [38], were used because of their model dependence [2]. In this article, we consider all the RMF parameter sets which satisfy the above bounds and also consistent with observational bound on the maximum mass, i.e. $M_{\max} \geq 1.97 M_{\odot}$.

2.2 Quark EOS

To construct the EOS of quark matter, we adopt the modified MIT Bag model that provides phenomenological description of the quark phase. The grand potential is given by [20,39]:

$$\Omega_{\mathrm{QM}} = \sum_i \Omega_i^0 + \frac{3\mu^4}{4\pi^2}(1 - a_4) + B_{\mathrm{eff}}, \tag{3}$$

where Ω_i^0 denotes the grand potentials of non-interacting Fermi gases of up (u), down (d) and strange (s) quarks and electrons. The other two terms in Eq. (3) correspond to the strong interaction correction and the non-perturbative QCD effects which are accounted via two effective parameters a_4 and B_{eff}, with $\mu (= \mu_u + \mu_d + \mu_s)$ being the baryon chemical potential of quarks.

We consider the phase transition from the nucleonic matter to the quark matter via Gibbs construction [1, 40] which is characterized by the appearance of a mixed phase of nucleonic and quark matter between the pure nucleonic and pure quark phases.

2.3 Tidal deformability

At the initial stage of an inspiraling binary NS, the tidal effect on a star can be written at linear order as [41]:

$$Q_{ij} = -\lambda \mathcal{E}_{ij}, \tag{4}$$

where Q_{ij} represents the induced quadrupole moment of the star and $\mathcal{E}_{ij}$ is assumed to be the external static tidal field exerted by the partner. The parameter λ is related to the dimensionless quadrupole tidal love number k_2 as ($G = c = 1$)

$$\begin{aligned} \lambda &= \frac{2}{3} k_2 R^5, \\ \Lambda &= \lambda / M^5, \end{aligned} \tag{5}$$

where Λ is the dimensionless tidal deformability.

We follow the framework developed by Hinderer and collaborators [16,41] to calculate k_2 and subsequently Λ. The value of k_2 depends on the EOS and lies in the range $\simeq 0.05 - 0.15$ [16]. This quantity can be expressed in terms of $C = M/R$, the compactness parameter as

$$\begin{aligned} k_2 = \frac{8C^2}{5}(1-2C)^2[2 + 2C(y-1) - y] \\ \times \{2C[6 - 3y + 3C(5y-8)] \\ + 4C^3[13 - 11y + C(3y-2) + 2C^2(1+y)] \\ + 3(1-2C)^2[2 - y + 2C(y-1)]\ln(1-2C)\}^{-1}, \end{aligned} \tag{6}$$

where y is defined as $y \equiv y(r)|_{r=R}$. The function $y(r)$ can be obtained by solving the following first-order differential equation:

$$r\frac{\mathrm{d}y}{\mathrm{d}r} + y(r)^2 + y(r)e^{\lambda(r)}\left\{1 + 4\pi r^2\left[p(r) - \varepsilon(r)\right]\right\} + r^2 Q(r) = 0, \tag{7}$$

with

$$\begin{aligned} Q(r) = 4\pi e^{\lambda(r)}\left[5\varepsilon(r) + 9p(r) + \frac{\varepsilon(r) + p(r)}{\mathrm{d}p/\mathrm{d}\varepsilon}\right] \\ - 6\frac{e^{\lambda(r)}}{r^2} - \left(\frac{\mathrm{d}\nu}{\mathrm{d}r}\right)^2, \end{aligned} \tag{8}$$

$$e^{\lambda(r)} = \left[1 - \frac{2m(r)}{r}\right], \qquad \frac{\mathrm{d}\nu}{\mathrm{d}r} = \frac{2}{r}\left[\frac{m(r) + 4\pi p(r) r^3}{r - 2m(r)}\right] \tag{9}$$

and boundary condition $y(0) = 2$. Given an EOS and the central pressure $p(0)$, the Love number and the tidal deformability can be obtained by solving Eq. (7) together with the Tolman–Oppenheimer–Volkoff (TOV) equations [1]:

$$\frac{\mathrm{d}p}{\mathrm{d}r} = -\frac{\left[p(r) + \varepsilon(r)\right]\left[m(r) + 4\pi r^3 p(r)\right]}{r[r - 2m(r)]} \tag{10}$$

$$m(r) = 4\pi \int_0^r \varepsilon(r) r^2 \,\mathrm{d}r. \tag{11}$$

3 Results and discussion

We construct an EOS with nucleon-quark phase transition via Gibbs construction. For the nucleonic part, we consider all the RMF EOSs which are consistent with both the latest saturation properties as given in Eq. (2) and the observational lower bound on maximum mass $M_{\rm max} \geq 1.97 M_\odot$. In Table 1, we list all the nucleonic EOSs considered here along with their saturation properties and maximum mass. Since the choice of the crustal EOS does not significantly affect the NS observables [52], we employ the Baym–Pethick–Sutherland (BPS) EOS [53]. The crust–core matching is modeled in a thermodynamics consistent fashion by following Ref. [54]. Also tabulated are the values of tidal deformabilities for a $1.4M_\odot$ NS calculated using Eq. (5). It is seen that only three EOSs, namely HC, TW99 and NLρ are consistent with the tidal deformability bound $\Lambda_{1.4} \leq 580$ as also found in Ref. [26].

We generate a large number of quark matter EOSs corresponding to different values of $B_{\rm eff}^{1/4}$ and a_4 given in Eq. (3). These EOSs are then combined with all the nucleonic EOSs considered via the Gibbs construction. However, we discard EOSs for which the starting density of mixed phase is smaller than the crust–core transition density.

Figure 1 shows the maximum masses as a function of the Bag parameter $B_{\rm eff}^{1/4}$ for all the EOSs with a nucleon-quark phase transition obtained with values of $a_4 = 0.5$ (left panel) and 0.6 (right panel). The results for the EOS BKA22 are not shown as it gives a star with maximum mass of $1.97M_\odot$, and further addition of quarks makes the EOS softer leading to a $M_{\rm max}$ below the observed bound. Note that different EOSs within a family are obtained by varying the single parameter, namely α_3' for S271 and NL3v and α_2' [47,48] for NL3$\sigma\rho$ (see Eq. (1)) that provides different symmetry energy behavior without affecting the $M_{\rm max}$, as can be seen from Table 1. For each of these three families, we only display results corresponding to the highest and lowest values of the parameter; the results for the other parameters fall in between these two limits.

At a fixed a_4, a small $B_{\rm eff}$ leads to a stiffer quark matter EOS as evident from Eq. (3) and noting that $P = -\Omega_{QM}$. This causes the onset of phase transition i.e. the mixed phase to occur early at a lower density and also of wider extent, resulting in softening of the overall nucleon-quark EOS and generating star with smaller $M_{\rm max}$. With increasing $B_{\rm eff}$, the quark phase has a smaller effect on the overall EOS due to its delayed appearance which causes the $M_{\rm max}$ to increase and eventually gives maximum mass for pure nucleonic star. Obviously, the effect is enhanced for much stiffer quark matter EOS for large values of a_4.

It is evident from Fig. 1 (right panel) that pure nucleonic EOS, viz FSUGarnet, TW99 and NLρ which have maximum mass slightly above $2M_\odot$ (i.e. $M_{\rm max} < 2.10M_\odot$) cannot support stars with a maximum mass of $1.97M_\odot$ when quark phase is included with parameter value $a_4 = 0.6$. While nucleon-quark stars in FSUGarnet and TW99 fail to satisfy the maximum bound for smaller values of Bag parameter, the failure in NLρ EOS is for the entire range of $B_{\rm eff}^{1/4}$ studied here. All the other 17 EOSs for $a_4 = 0.6$ value are found consistent with the maximum mass bound for the whole range of $B_{\rm eff}$. In contrast, for $a_4 = 0.5$ (left panel), all the stars with nucleon-quark phase transition satisfy the maximum mass bound. By increasing the a_4 value to 0.6 and beyond causes more and more EOSs to fail the maximum mass constraint. This is because the quark EOS becomes stiffer with increasing a_4 as discussed above.

We now present results for the tidal deformability of neutron stars with nucleon-quark phase transition following the prescription presented in Sect. 2.3. With increasing Bag constant, since the stiffer EOS generates stars with larger radii as well, the tidal deformability bound of will not be satisfied for large values of $B_{\rm eff}$. In Table 2, we show the maximum values of $B_{\rm eff}^{1/4}$ corresponding to different nucleonic EOSs, for which the tidal deformability bound of $\Lambda_{1.4} \leq 580$ is satisfied by $1.4M_\odot$ neutron star [15]. These maximum values of $B_{\rm eff}^{1/4}$ are marked with "crosses" in Fig. 1. The curves corresponding to nucleonic EOS, DDME2, NL3$\sigma\rho$3, NL3$\sigma\rho$6, NL3v3, NL3v6, BSR1-5 with $a_4 = 0.5$ and NL3$\sigma\rho$6 and NL3v6 with $a_4 = 0.6$ are not marked with any cross as these EOSs are unable to satisfy the $\Lambda_{1.4} \leq 580$ bound for any value of $B_{\rm eff}^{1/4}$. On the other hand, TW99, HC and NLρ EOSs satisfy the $\Lambda_{1.4}$ constraint for pure nucleonic stars. Since the inclusion of quarks makes the overall EOS softer resulting in stars with smaller masses and radii, the bounds are naturally satisfied for all values of $B_{\rm eff}^{1/4}$ and hence these EOSs with nucleon-quark phase are not marked with any cross. It is interesting to note that out of the 17 pure nucleonic EOSs that are not consistent with the tidal deformability constraint, 15 EOSs (except NL3$\sigma\rho$6 and NL3v6) for a range of values of $B_{\rm eff}$ and a_4 can generate neutron stars with quark phase that are consistent with the bound. However, the tidal deformability bound is found to severely constrain the quark matter parameter space $(B_{\rm eff}^{1/4}, a_4)$, irrespective of the nucleonic EOS.

The strong correlation between $\Lambda_{1.4}$ and $R_{1.4}$, as expected due to $\Lambda \propto R^5$, has been explored within various nuclear model approaches (without quarks) [17,18,55–57]. For all the RMF EOSs considered here and pure-nucleon stars, we obtained [26] the relation $\Lambda_{1.4} = 1.53 \times 10^{-5} (R_{1.4}/{\rm km})^{6.83}$, with maximum deviation $|(\Lambda_{1.4}^{\rm fit} - \Lambda_{1.4})/\Lambda_{1.4}|$ of $\sim 8\%$. The extra factor of 1.83 in the exponent stems from the quadrupole love number k_2 which depends on the EOS and, therefore, on the radius of the star in a complicated fashion (see Sect. 2.3). In Fig. 2, we present the correlation between $\Lambda_{1.4}$ and $R_{1.4}$ using these nucleonic EOSs and incorporating nucleon-quark phase transition. We find that the strong $\Lambda_{1.4}-R_{1.4}$ correlation observed for pure nucleonic stars still persists with phase transition which can be fitted as $\Lambda_{1.4} = 5.22 \times 10^{-5} (R_{1.4}/{\rm km})^{6.35}$. However, the correlations with quark phase have a slightly more spread, the maximum deviation is $\sim 16\%$. Using this

Table 1 Various relativistic nuclear mean-field models and their nuclear matter saturation properties, namely incompressibility K, symmetry energy J and its slope L

EOS	K (MeV)	J (MeV)	L (MeV)	$M_{\max}/M_\odot$	$\Lambda_{1.4}$	$R_{1.4}$ (km)
FSUGarnet [42]	229.5	30.9	51.0	2.07	638	12.95
HC [43]	231.9	31.0	58.5	2.28	440	12.26
DDME2 [44]	250.9	32.3	51.3	2.48	705	13.02
DD2 [35]	242.7	31.7	55.0	2.42	684	13.16
TW99 [34]	240.3	32.8	55.3	2.08	403	12.29
DDME1 [45]	244.7	33.1	55.5	2.44	674	13.16
DD [46]	240.0	31.6	56.0	2.41	679	13.15
$NL3\sigma\rho6$ [47]	270.0	31.5	55.0	2.75	974	13.78
$NL3\sigma\rho5$ [47]	270.0	32.3	61.0	2.75	986	13.83
$NL3\sigma\rho4$ [47]	270.0	33.0	68.0	2.75	1002	13.91
$NL3\sigma\rho3$ [47]	270.0	33.9	76.0	2.75	1027	14.01
NL3v6 [48]	271.6	32.4	61.1	2.75	948	13.77
NL3v5 [48]	271.6	33.2	68.2	2.75	965	13.84
NL3v4 [48]	271.6	34.0	77.0	2.75	992	13.95
NL3v3 [48]	271.6	34.5	82.1	2.74	1012	14.01
S271v6 [48]	271.0	32.7	59.8	2.35	629	13.05
S271v5 [48]	271.0	33.3	65.4	2.34	643	13.12
S271v4 [48]	271.0	33.8	71.8	2.34	663	13.23
S271v3 [48]	271.0	34.4	78.9	2.34	694	13.35
S271v2 [48]	271.0	35.0	86.9	2.34	742	13.51
BSR1 [32]	239.9	31.0	59.4	2.47	797	13.42
BSR2 [32]	239.9	31.5	62.0	2.39	751	13.34
BSR3 [32]	230.6	32.7	70.5	2.36	751	13.39
BSR4 [32]	238.6	33.2	73.2	2.44	790	13.49
BSR5 [32]	235.8	34.5	83.4	2.48	838	13.67
IOPB-I [49]	222.7	33.3	63.6	2.15	688	13.27
BKA22[50]	225.2	33.2	78.8	1.97	667	13.29
NLρ [51]	240.8	30.4	84.6	2.09	571	12.81

For these nuclear RMF models, some important observational properties are presented, namely the maximum mass of neutron star $M_{\max}$, the radii $R_{1.4}$ and tidal deformability $\Lambda_{1.4}$ of a $1.4M_\odot$ mass neutron star

Table 2 Listed for various nucleonic EOSs are the maximum values of $B_{\rm eff}^{1/4}$ that are consistent with the upper bound on $\Lambda_{1.4} \leq 580$ for the parameter values $a_4 = 0.5$ and 0.6 of Eq. (3)

Hadronic EOS	$B_{\rm eff}^{1/4}\|_{\max}$		$R_{1.4}$(km)		$(\Delta M_{\rm Q}/M_\odot)_{\max}$
	$a_4 = 0.5$	$a_4 = 0.6$	$a_4 = 0.5$	$a_4 = 0.6$	
FSUGarnet	153	163	12.783	12.800	0.00
DDME2	NA	156	NA	12.863	0.02
DD2	146	158	12.821	12.892	0.01
DDME1	147	158	12.851	12.882	0.01
DD	146	158	12.808	12.878	0.01
NL3$\sigma\rho$6	NA	NA	NA	NA	0.13
NL3$\sigma\rho$3	NA	146	NA	12.518	0.17
NL3v6	NA	NA	NA	NA	0.14
NL3v3	NA	146	NA	12.520	0.16
S271v6	154	163	12.923	12.916	0.00
S271v2	152	162	13.049	13.064	0.00
BSR1	NA	155	NA	12.835	0.02
BSR2	NA	158	NA	12.901	0.00
BSR3	NA	160	NA	12.966	0.00
BSR4	NA	158	NA	12.967	0.02
BSR5	NA	157	NA	12.971	0.02
IOPB-I	152	162	12.979	12.994	0.00

The corresponding radii $R_{1.4}$ of a $1.4M_\odot$ star are given. NA denotes that No Allowed value of $B_{\rm eff}^{1/4}$ is consistent with the bound. The last column gives the maximum mass of the pure quark part (see text for details)

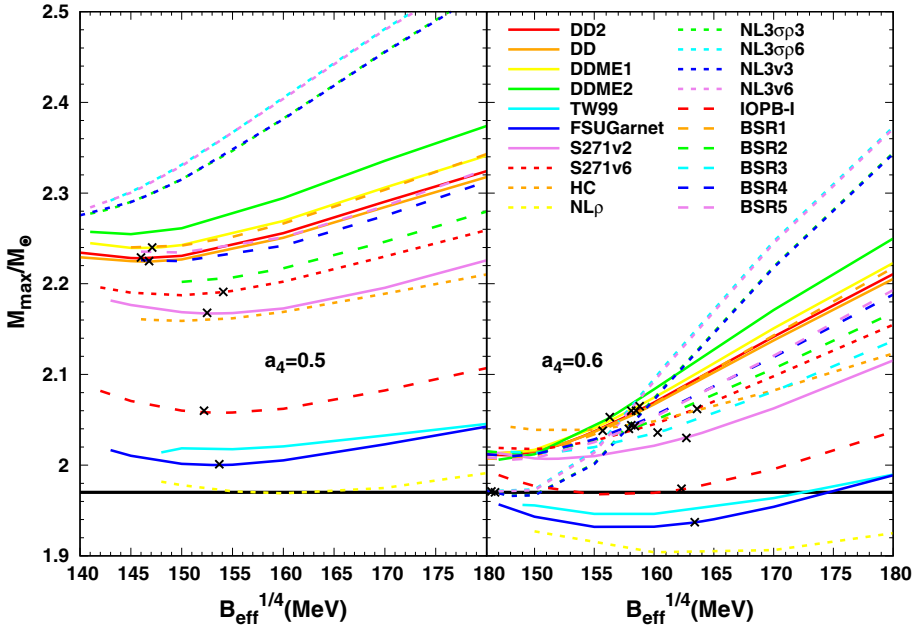

Fig. 1 Maximum masses of neutron stars with nucleon-quark phase transition as a function of Bag pressure $B_{\rm eff}^{1/4}$ for $a_4 = 0.5$ (left panel) and $a_4 = 0.6$ (right panel) of Eq. (3) for various nucleonic EOSs as listed in Table 1. The black thick horizontal line represents the lower bound $M_{\rm max} = 1.97 M_\odot$ on maximum mass. Crosses indicate maximum value of $B_{\rm eff}^{1/4}$ for stars that are consistent with $\Lambda_{1.4} \leq 580$ bound

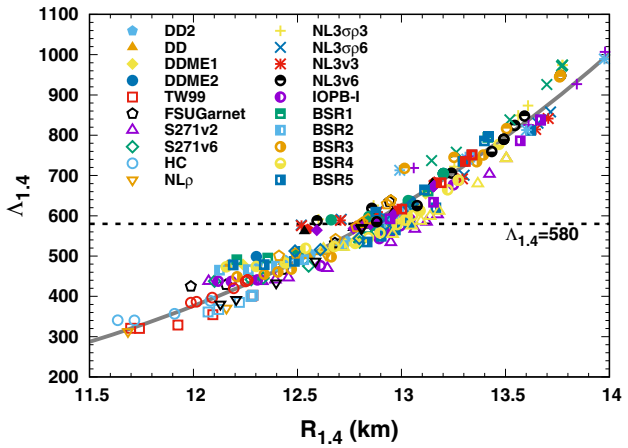

Fig. 2 Correlation between $\Lambda_{1.4}$ and R_{14} for EOS with nucleon-quark phase transition constructed from different nuclear EOSs and for a range of Bag parameter values $B_{\rm eff}^{1/4} \sim 145{-}180$ MeV and $a_4 = 0.5$ and 0.6. The dashed line represents the upper bound on $\Lambda_{1.4}$ given by GW170817 [25] and the solid line is for the fit $\Lambda_{1.4} = 5.22 \times (R_{14}/{\rm km})^{6.35}$

fit function and the upper bound on $\Lambda_{1.4} \leq 580$, we obtain an approximate upper bound on the radius of $R_{1.4} \leq 12.9$ km. Interestingly, the same bound was obtained on $R_{1.4}$ for nucleon-only stars constructed from the RMF EOSs [26].

In Fig. 3, we show the volume fraction χ of quarks for the maximum mass configurations corresponding to different Bag parameters $B_{\rm eff}^{1/4}$ and values of $a_4 = 0.5$ and 0.6. Only the EOSs of Fig. 1, that satisfy the maximum mass bound for the quark matter parameters used, are considered here. The cross indicate the maximum values of $B_{\rm eff}^{1/4}$ for which the corresponding EOS is consistent with the $\Lambda_{1.4} \leq 580$ bound. (NL3$\sigma\rho$6 and NL3v6 are not shown as these cannot support $\Lambda_{1.4} \leq 580$.) We observe that with increasing $B_{\rm eff}$, the fraction of quarks in the star decreases. This can be explained from the fact that larger $B_{\rm eff}$ makes the quark EOS softer which delays the appearance of mixed phase to a higher density. Consequently, the overall EOS becomes stiffer resulting in higher maximum mass for a neutron star but at a lower central density (see Fig. 1).

In the mixed phase, the quark fraction increases from $\chi = 0$ (pure nucleonic phase) to $\chi = 1$ (pure quark phase) as the density increase. Since the maximum density inside the star is lower for a higher $B_{\rm eff}$, the corresponding quark fraction is also smaller. Figure 3 reveals that for $a_4 = 0.6$ there are several RMF models for which the neutron star core can have pure quark matter while satisfying the $\Lambda_{1.4} \leq 580$ constraint, whereas, for $a_4 = 0.5$, no such EOS exists that permits a pure quark matter core. Instead, the neutron star core consists of a mixed phase of nucleons and quarks. In Table 2, we have also listed the maximum masses of the pure quark phase star $(\Delta M_{\rm Q})_{\rm max}$. For a given RMF EOS, each combination of the parameters $(B_{\rm eff}^{1/4}, a_4)$ defines a value of $\Delta M_{\rm Q} = M_{\rm max} - M_{\rm mp}$, where $M_{\rm mp}$ is the mass of the star with the end point of the mixed phase as the central density. $(\Delta M_{\rm Q})_{\rm max}$ then corresponds to the maximum value of $\Delta M_{\rm Q}$ obtained by considering all possible combinations of $(B_{\rm eff}^{1/4}, a_4)$. From Table 2, we find

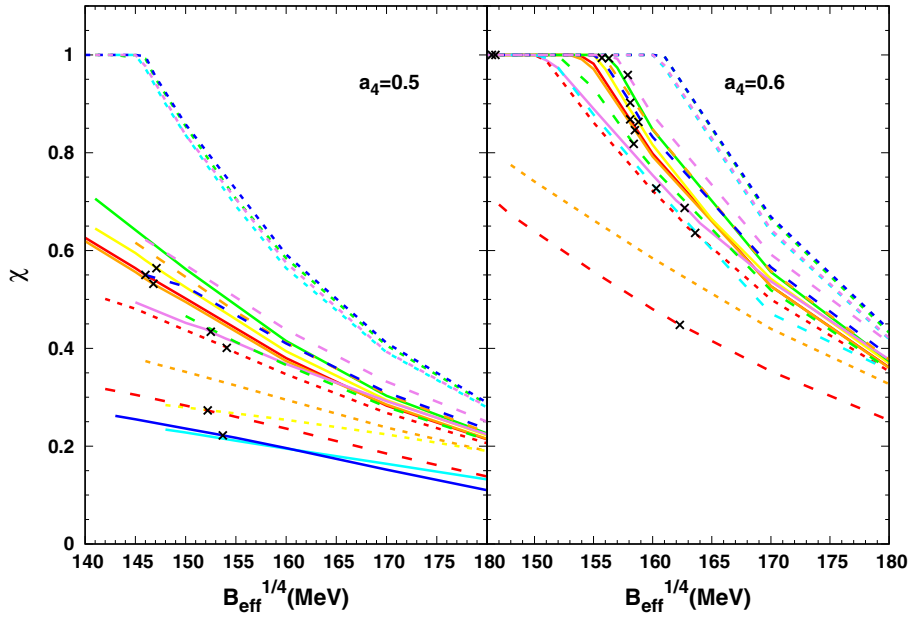

Fig. 3 Volume fraction of quarks χ corresponding to maximum mass configuration as a function of $B_{\rm eff}^{1/4}$ for $a_4 = 0.5$ (left panel) and $a_4 = 0.6$ (right panel) for different nucleonic EOSs. The line styles and crosses are same as in Fig. 1 for the various EOS

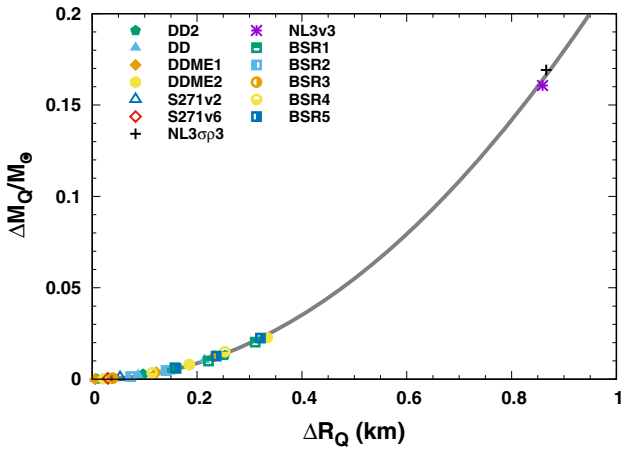

Fig. 4 Masses and radii of quark cores for the maximum mass neutron star configurations corresponding to different nucleonic EOSs and Bag model parameters that are consistent with $M_{\rm max} \geq 1.97 M_\odot$ and $\Lambda_{1.4} \leq 580$ bounds. The thick grey line represents the fit $\Delta M_Q/M_\odot = 0.22 \times (\Delta R_Q/{\rm km})^{2.01}$

that NL3$\sigma\rho$3 and NL3v3 EOSs have appreciable size of quark-matter core with mass of $\sim 0.17 M_\odot$ which corresponds to $\sim 8\%$ of total mass of the star. For other EOSs the quark core mass is quite small up to $0.02 M_\odot$.

In Fig. 4, we display the variation of masses ΔM_Q with the radii ΔR_Q of the quark-matter core for the maximum mass neutron star configurations corresponding to different RMF nucleonic EOS and Bag model parameters. We show only those configurations which are consistent with both the maximum mass bound and the tidal deformability bound. In the present model analysis, while the maximum mass of $0.17 M_\odot$ predicted for the quark-matter core is confined within a radius 0.9 km, the majority of the models lead to a much smaller masses and radii of $\sim 0.02 M_\odot$ and ~ 0.3 km. It is interesting to observe that the mass and radius of the quark core are strongly correlated and can be fitted as $\Delta M_Q/M_\odot = 0.22 \times (\Delta R_Q/{\rm km})^{2.01}$. We note that the central densities of these quark core stars are found early in the pure quark phase, immediately after the mixed phase, instead at very high densities where all the quark EOSs have the same speed of sound ($c_s^2 = 1/3$). However, we found that speed of sound for these quark core stars are nearly similar which result in a strong correlation between ΔM_Q and ΔR_Q. Nevertheless, it may be worth investigating where other model approaches lead to such a tight correlation in ΔM_Q and ΔR_Q.

4 Conclusions

Observation of $\sim 2 M_\odot$ neutron stars and the measurement of tidal deformability from GW170817 have posed serious challenge to the construction of EOS of a neutron star. While the maximum mass bound enforces a stiff EOS, the tidal deformability bound $\Lambda_{1.4} \leq 580$ demands a soft EOS. A natural way to account such a behavior is by incorporating a nucleon-quark phase transition in the EOS at higher densities. In this work, we have investigated this possibility by considering nucleonic EOS from several RMF models, that are compatible with constraints imposed by experimental data and observations, and including a quark matter EOS (via Bag model) by exploring a wide range of quark matter parameter space. The EOSs with phase transition are generated via Gibbs construction character-

ized by nucleon-quark mixed phase. We have shown that most of the nuclear EOSs that do not satisfy the tidal deformability bound, become consistent with this bound when transition to quark-matter is included for a rather large combination of Bag model parameters $(B_{\rm eff}, a_4)$. However, the tidal deformability constraint is found to significantly reduce the allowed region of quark matter parameter space, regardless of the nucleonic EOS. We find that, for most of the nucleonic models studied, the neutron star core contains a mixed phase of nucleons and quarks. We also find that several EOSs can support a neutron star with a pure quark matter core, albeit with quite small quark core mass within the range of $\sim (0.02-0.17)M_{\odot}$. Furthermore, we showed that a strong correlation exists between the masses and radii of the quark matter core.

Apart from the three RMF nucleonic EOSs found in this study, there are few other nucleonic EOSs (e.g. APR [58], SLy [59]) which are consistent with the two solar mass and tidal deformability bounds. Therefore, it is quite difficult to distinguish purely nucleonic stars from hybrid stars with small quark core and/or mixed phase, observationally. Nevertheless, recent binary neutron star simulations [60] have shown that in the so-called delayed phase transition scenario a hypermassive hybrid star can be formed. During this process, the emitted gravitational wave can provide signature of hybrid stars even with a mixed phase. However, the signature is strong for stars with significant quark core. The present study may thus be quite promising in the search for hybrid stars.

References

1. N.K. Glendenning, *Compact Stars, Nuclear Physics, Particle Physics, and General Relativity*, 2nd edn. (Springer, New York, 2000)
2. M. Oertel, M. Hempel, T. Klähn, S. Typel, Rev. Mod. Phys. **89**, 015007 (2017)
3. J.M. Lattimer, M. Prakash, Phys. Rep. **442**, 109 (2007)
4. L. Lindblom, Astrophys. J. **398**, 569 (1992)
5. P. Demorest, T. Pennucci, S. Ransom, M. Roberts, J. Hessels, Nature **467**, 1081 (2010)
6. E. Fonseca et al., Astrophys. J. **832**, 167 (2016)
7. J. Antoniadis et al., Science **340**, 6131 (2013)
8. H.T. Cromartie et al., Nat. Astron. **4**(1), 72 (2019)
9. S. Guillot, M. Servillat, N.A. Webb, R.E. Rutledge, Astrophys. J. **772**, 7 (2013)
10. F. Özel, D. Psaltis, T. Guver, G. Baym, C. Heinke, S. Guillot, Astrophys. J. **820**(1), 28 (2016)
11. F. Özel, P. Freire, Ann. Rev. Astron. Astrophys. **54**, 401 (2016)
12. J. Nättilä, M. Miller, A. Steiner, J. Kajava, V. Suleimanov, J. Poutanen, Astron. Astrophys. **608**, A31 (2017)
13. T.E. Riley et al., Astrophys. J. Lett. **887**, L21 (2019)
14. M.C. Miller et al., Astrophys. J. Lett. **887**, L24 (2019)
15. B.P. Abbott et al. (LIGO Scientific and Virgo Collaborations), Phys. Rev. Lett. **119**(16), 161101 (2017)
16. T. Hinderer, B.D. Lackey, R.N. Lang, J.S. Read, Phys. Rev. D **81**, 123016 (2010)
17. F.J. Fattoyev, J. Piekarewicz, C.J. Horowitz, Phys. Rev. Lett. **120**(17), 172702 (2018)
18. E. Annala, T. Gorda, A. Kurkela, A. Vuorinen, Phys. Rev. Lett. **120**(17), 172703 (2018)
19. E.R. Most, L.R. Weih, L. Rezzolla, J. Schaffner-Bielich, Phys. Rev. Lett. **120**(26), 261103 (2018)
20. R. Nandi, P. Char, Astrophys. J. **857**(1), 12 (2018)
21. N.B. Zhang, B.A. Li, J. Xu, Astrophys. J. **859**(2), 90 (2018)
22. B. Margalit, B.D. Metzger, Astrophys. J. **850**, L19 (2017)
23. L. Rezzolla, E.R. Most, L.R. Weih, Astrophys. J. Lett. **852**, L25 (2018)
24. M. Shibata, S. Fujibayashi, K. Hotokezaka, K. Kiuchi, K. Kyutoku, Y. Sekiguchi, M. Tanaka, Phys. Rev. D **96**(12), 123012 (2017)
25. B.P. Abbott et al. (LIGO Scientific and Virgo Collaborations), Phys. Rev. Lett. **121**(16), 161101 (2018)
26. R. Nandi, P. Char, S. Pal, Phys. Rev. C **99**(5), 052802 (2019)
27. J.D. Walecka, Ann. Phys. **83**, 491 (1974)
28. J. Boguta, A.R. Bodmer, Nucl. Phys. A **292**, 413 (1977)
29. Y. Sugahara, H. Toki, Nucl. Phys. A **579**, 557 (1994)
30. B.D. Serot, J.D. Walecka, Int. J. Mod. Phys. E **6**, 515 (1997)
31. C.J. Horowitz, J. Piekarewicz, Phys. Rev. Lett. **86**, 5647 (2001)
32. S.K. Dhiman, R. Kumar, B.K. Agrawal, Phys. Rev. C **76**, 045801 (2007)
33. M. Dutra et al., Phys. Rev. C **90**(5), 055203 (2014)
34. S. Typel, H.H. Wolter, Nucl. Phys. A **656**, 331 (1999)
35. S. Typel, G. Ropke, T. Klahn, D. Blaschke, H. Wolter, Phys. Rev. C **81**, 015803 (2010)
36. P. Reinhard, Rep. Prog. Phys. **52**, 439 (1989)
37. J. Piekarewicz, Phys. Rev. C **69**, 041301 (2004)
38. S. Shlomo, V.M. Kolomietz, G. Colò, Eur. Phys. J. A **30**, 23 (2006)
39. S. Weissenborn, I. Sagert, G. Pagliara, M. Hempel, J. Schaffner-Bielich, Astrophys. J. **740**, L14 (2011)
40. N.K. Glendenning, Phys. Rev. D **46**, 1274 (1992)
41. T. Hinderer, Astrophys. J. **677**, 1216 (2008)
42. R. Utama, W. Chen, J. Piekarewicz, J. Phys. G **43**(11), 114002 (2016)
43. J.K. Bunta, S. Gmuca, Phys. Rev. C **68**, 054318 (2003)
44. G. Lalazissis, T. Niksic, D. Vretenar, P. Ring, Phys. Rev. C **71**, 024312 (2005)
45. T. Niksic, D. Vretenar, P. Ring, Phys. Rev. C **66**, 064302 (2002)
46. S. Typel, Phys. Rev. C **71**, 064301 (2005)
47. H. Pais, C. Providência, Phys. Rev. C **94**(1), 015808 (2016)
48. C. Horowitz, J. Piekarewicz, Phys. Rev. C **66**, 055803 (2002)
49. B. Kumar, B. Agrawal, S. Patra, Phys. Rev. C **97**(4), 045806 (2018)
50. B. Agrawal, Phys. Rev. C **81**, 034323 (2010)
51. B. Liu, V. Greco, V. Baran, M. Colonna, M. Di Toro, Phys. Rev. C **65**, 045201 (2002)
52. B. Biswas, R. Nandi, P. Char, S. Bose, Phys. Rev. D **100**(4), 044056 (2019)

53. G. Baym, C. Pethick, P. Sutherland, Astrophys. J. **170**, 299–317 (1971)
54. M. Fortin, C. Providencia, A. Raduta, F. Gulminelli, J.L. Zdunik, P. Haensel, M. Bejger, Phys. Rev. C **94**(3), 035804 (2016)
55. I. Tews, J. Margueron, S. Reddy, Eur. Phys. J. A **55**(6), 97 (2019)
56. S. De, D. Finstad, J.M. Lattimer, D.A. Brown, E. Berger, C.M. Biwer, Phys. Rev. Lett. **121**(9), 091102 (2018)
57. T. Malik, N. Alam, M. Fortin, C. Providência, B. Agrawal, T. Jha, B. Kumar, S. Patra, Phys. Rev. C **98**(3), 035804 (2018)
58. A. Akmal, V.R. Pandharipande, D.G. Ravenhall, Phys. Rev. C **58**, 1804–1828 (1998)
59. F. Douchin, P. Haensel, Astron. Astrophys. **380**, 151 (2001)
60. L.R. Weih, M. Hanauske, L. Rezzolla, Phys. Rev. Lett. **124**(17), 171103 (2020)